Available online at www.sciencedirect.com

ScienceDirect

journal homepage: http://www.elsevier.com/locate/acme

Original Research Article

Prediction model of long-term prestress loss interaction for prestressed concrete containment vessels

Ahmad Shokoohfar, Alireza Rahai *

Department of Civil Engineering, Amirkabir University of Technology, Hafez, Tehran 158754413, Islamic Republic of Iran

ARTICLE INFO

Article history:
Received 3 April 2016
Accepted 24 September 2016
Available online 20 October 2016

Keywords:
Creep
Shrinkage
Stress relaxation
Concrete containment
Interaction

ABSTRACT

Conventional methods disregard the interaction effects between concrete creep and tendon relaxation to evaluate the long-term prestressed losses. The main contribution of this paper is to present a new method to compute this interaction for prestressed concrete containment vessels. A time-dependent numerical study is conducted to compare long-term prestress losses in different prediction models. A prestress loss test program is conducted to validate the numerical analysis method for a concrete containment vessel. To perform a more comprehensive numerical study, various variables such as radius to water height ratios (R/H), tendon material (improved or normal relaxation), and different constant temperature conditions are considered in the analysis models. The obtained analytical results are categorized into three classes: creep and shrinkage losses, stress relaxation losses and simultaneous long-term losses. The analytical results show that the (R/H) ratios have no significant effects on long-term prestress loss. Nevertheless, the other investigated variables have impressive effects on the long-term loss evaluation. The analytical results are used to calculate the interaction coefficients, which demonstrate the interaction between concrete creep losses and tendon relaxation. Eventually, the interaction coefficient data are expressed as a function of stress relaxation loss to creep and shrinkage loss ratio.

1. Introduction

Time-dependent behavior of concrete structures has been of interest to engineers for decades. Long-term prestress loss prediction is one of the most common applications of time-dependent analysis of the structures. It comprises concrete creep and shrinkage and tendon stress relaxation. Several methods have been developed to predict the prestress loss due to creep in hardened concrete. The age adjusted effective modulus method (AAEM) is the most known methods for creep prestress loss prediction [1,2]. ACI-209-92, CEB-MC90-99, Bazant B3 and CEB-fib-2010 [3–7] prediction models of creep were developed based on AAEM. Bazant et al. [8] improved the

* *Corresponding author.*
E-mail address: rahai@aut.ac.ir (A. Rahai).
http://dx.doi.org/10.1016/j.acme.2016.09.002

AAEM estimations by the innovation of a long-term relaxation function from the compliance function of aging concrete. Francis and Si [9] presented a new relaxation model for steel tendons based on the equivalent creep coefficient to enable the accurate estimation of tendon prestressing losses. Lundqvist and Nilsson [10] compared the international codes prediction with Swedish prestressed containment inspection data. Based on their investigations, ACI-209-92 and CEB-MC90-99 provides the most precise prediction of the prestressing force losses for circular containment vessels. Hsuan and Lin [11] studied the behavior of PWR prestressed containment vessels by considering the time dependent prestressing losses. The analytical results of their study show that the prestressed tendons have been lost about 19 percent of their initial values after 40 years. The previous prediction models were presented long-term prestress losses based on the superposition principle. This issue led to overestimate the loss prediction because of the concrete creep and tendon relaxation interaction effects. In this study, a time dependent numerical study is performed to estimate the long-term prestress loss calculation procedure by means of a new interaction model in prestressed containments. The numerical study verification is performed using the experimental data obtained from the concrete containment model which is constructed at Amirkabir University of Technology (AUT).

2. Research significance

The prestressed concrete containment vessels utilized for so many purposes include water refinery systems, nuclear reactor protection structure and LNG (liquefied natural gas) containments. The primary reasons to apply the prestressed concrete in vessels are to improve the safety level and material consumption optimization. But the main problems which limit the use of prestressed systems are the complicated construction practice and the prestress loss control in the containment vessel lifetime. The majority of the concrete design codes present different algorithms and prediction models to estimate the prestress loss value, without considering these procedures, over-design of the prestressed structures is inevitable. Otherwise, the long-term prestress loss causes to reduce the reliability of some cases such as PWR (pressurized water reactor) and the LNG containment vessels. Therefore, it is so important to investigate new procedures to refine the long-term prestress loss prediction models.

3. Numerical model features

The numerical models were designated for three ratios of radius to maximum water height (R/H = 2, 3 and 4) based on ACI design code [12] and using SAP 2000 Software [13]. At first, the structure of storage tank was modeled by shell elements without any prestressed or non-prestressed reinforcement. The mesh size is variable due to the R/H ratio and range from 275 mm × 1120 mm to 275 mm × 2240 mm for walls. The foundation square element size varies from 930 to 1550 mm. The hydrostatic and hydrodynamic loading was considered in the models. The hydrodynamic load is assigned according to ASCE 7-16 [14] for site class B, site-specific design spectra of Tehran northern area and occupancy category (I). The soil springs were assigned to the foundation shell elements according to ASCE 41-13 [15] for site class B. An assumed residual radial compression due to prestressing effects was added to the SAP 2000 analysis results based on factored load combinations of ACI design code. The vertical and circumferential tendons were dimensioned based on reference [16]. As the secondary design procedure, tendon truss elements were added to model to check the service limit based on the allowable stress recommended by ACI design code and design the non-prestressed reinforcement. Eventually, the obtained details of the structure were stimulated using ABAQUS software [17].

Geometric properties of the models and its depicted features are present in Fig. 1 and Table 1, respectively. In addition, reinforcement details of the models are given in Table 2 in accordance to containment foundation zones.

Table 3 provides the prestressed properties according to the wall zones (see Fig. 1). Hydrostatic pressure was applied to the inner surface of the containment vessels. The temperature was increased from 20 °C to 55 °C to consider thermal effects in the numerical models. The walls and foundation are integrated and soil structure interaction (SSI) is ignored.

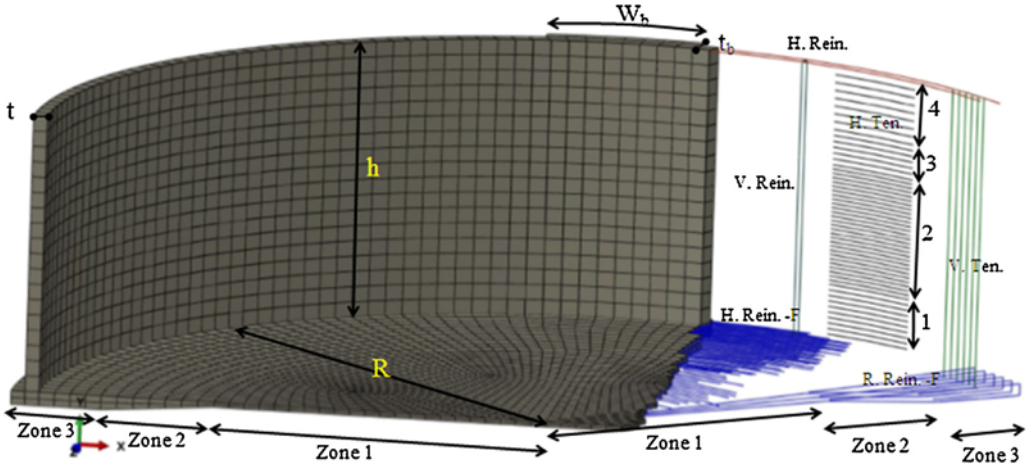

Fig. 1 – Main geometric features and mesh size of the FE models in the ABAQUS software [17].

Table 1 – Geometric properties.

Models	Radius, R (m)	Height, h (m)	Wall thickness, t (mm)	Buttress width, W_b (mm)	Base ring width – Zone 1 (mm)	Zone 1 thickness (mm)	Zone 2 width (mm)
F1	10	5.5	275	3080	1500	275	2200
F2	15	5.5	275	4588	1500	275	2200
F3	20	5.5	275	6029	1500	275	2200

Table 2 – Non-prestressed reinforcement properties.

Models	Circumferential reinforcement (H.-Rein.)	Vertical reinforcement (V.-Rein.)	Radial reinforcement of foundation (R-Rein-F)			Hoop reinforcement of foundation (H-Rein-F)		
			Zone-1	Zone-2	Zone-3	Zone-1	Zone-2	Zone-3
F1-F2-F3	Φ10 @ 75 mm	Φ10 @ 75 mm	Φ16 @ 100 mm	Φ16 @ 200 mm	Φ12 @ 200 mm	Φ16 @ 100 mm	Φ16 @ 200 mm	Φ12 @ 200 mm

Table 3 – Prestressed tendon properties.

Models	Vertical tendons (V-Ten)	Hoop tendons (H-Ten)			
		Zone-1	Zone-2	Zone-3	Zone-4
F1	1/2″ @ 200 mm	No.[a]: 10 @ 110 mm	No.: 29 @ 85 mm	No.: 7 @ 117 mm	No.: 7 @ 157 mm
F2	1/2″ @ 175 mm	No.[a]: 8 @ 100 mm	No.[a]: 10 @ 80 mm	No.[a]: 26 @ 75 mm	No.[a]: 12 @ 80 mm
F3	1/2″ @ 175 mm	No.[a]: 12 @ 91 mm	No.[a]: 9 @ 77 mm	No.[a]: 33 @ 66 mm	No.[a]: 13 @ 77 mm

[a] Number of tendons placed at above mentioned distances.

4. Material properties

Table 4 tabulates concrete material properties. All given properties are influential to predict the long-term prestress losses in the various model codes. The concrete Poisson's ratio is assumed to be 0.15. The modulus of elasticity is reduced as a function of time for each time step of the analysis. In fact, this process is performed to consider the concrete aging effects on prestress losses due to creep.

The Poisson's ratio for both pre-stressed and non-pre-stressed reinforcing is 0.3. The modulus of elasticity for steel reinforcement and tendons are 200 GPa and 185 GPa, respectively. The yield stress value of reinforcing bars and tendons are 420 MPa and 1490 MPa. The thermal expansion coefficient is 1.2×10^{-5} 1/°C.

Table 4 – Concrete material properties.

28-day compressive strength	40 MPa
Relative humidity	70%
Curing time	7
Age at loading	14
Maximum aggregate size	20 mm
Cement type	I
Moisture content	205 kg/m^3
Cement content	409 kg/m^3
W/C; water to cement ratio	0.5
a/C; aggregate to cement ratio	4.23
Fine aggregate percentage	40%
Air content	2%
Slump	75 mm
Unit weight	2345 kg/m^3
Thermal expansion coefficient	9×10^{-6} 1/°C

5. Short term prestressing losses in numerical models

According to Sandia Laboratories structural failure mode test (SFMT) results, using an average value for prestressing force uniformly distributed along the tendon, led to the same results as implementing a variable prestressing distribution [18]. Subsequently, in this paper, after short-term prestressing loss reduction, the remaining prestressing force is assigned as an average value along the tendon length.

Short-term prestress losses are calculated using the following formulas [19]:

$$X > L \Rightarrow \Delta_1 = \frac{E_p \delta}{L} \tag{1}$$

$$X < L \Rightarrow \Delta_1 = \frac{E_p \delta}{X} \tag{2}$$

where:

$$X_{cir} = \sqrt{\frac{E_p \delta}{\left(\frac{2\mu\alpha}{b^2+K}\right) f_{pj}}} \tag{3}$$

Table 5 – Short-term losses.

	Model	P_k (kN)	Anchorage slip loss (kN)	Elastic shortening loss (kN)	Friction loss (kN)	Short-term losses (kN)	f_{pe} (MPa)
F1	Vertical	130.06	17.19	0.63	0.63	18.44	1201.49
	Circumferential	130.06	5.10	1.19	22.42	28.71	1091.004
F2	Vertical	130.06	17.19	0.63	0.63	18.44	1201.49
	Circumferential	130.06	4.22	1.20	24.17	29.59	1081.517
F3	Vertical	130.06	17.19	0.63	0.63	18.44	1201.49
	Circumferential	130.06	3.87	1.20	25.76	30.83	1068.112

$$X_{ver} = \sqrt{\frac{E_p \delta}{K f_{pj}}} \tag{4}$$

and:

$$\Delta_2 = \frac{1}{2}\frac{E_p}{E_c} f_{cg} \tag{5}$$

$$\Delta_3 = f_{pi}\left(1 - e^{(kx - \mu\alpha_1)}\right) \tag{6}$$

where parameters are described as E_p: tendon modulus of elasticity, δ: anchorage slip (5 mm), X_{ver}: anchorage slip effective length for vertical tendons, X_{cir}: anchorage slip effective length for circumferential tendons, L: tendon length, k: wobble coefficient (0.000001 1/mm), x: considered distance from jacking zone, μ: coefficient of friction between post-tensioned tendon and conduit (0.21 1/rad), α_1: tendon angle change in distance x, f_{pj}: jacking prestress, f_{pi}: initial prestress, f_{pe}: effective prestress, f_{cg}: initial prestress in concrete cross section centroid and E_c: concrete modulus of elasticity. Δ_1, Δ_2 and Δ_3 are the prestress losses due to anchorage slip, elastic shortening and friction. The anchorage slip effective length (formulas (3) and (4)) are derived from [19]. The short-term losses are also evaluated using the SAP 2000 software [13] to ensure the calculated results. Table 5 summarizes the results from the equations (1)–(6).

The main purpose of this study is to investigate the main variables affecting the long-term prestress loss. The calculation of the short-term losses is carried out using the SAP 2000 [13] because of its features for assigning the tendon loads. One can determine the short-term loss parameters such as curvature coefficient, wobble coefficient and anchorage set slip then obtain the mean short-term losses. Nonetheless, the long-term prestress loss parameters are so complicated than can be defined using the SAP 2000 software [13]. Therefore, powerful FE software like ABAQUS [17] with advance property modules is required to investigate the long-term prestress losses.

6. Long-term prestress losses

Various parameters play pivotal roles in long-term prestress loss reduction. In this study, the dimensional proportion (R/H = 2, 3 and 4), temperature (20–55 °C) and tendon material (normal or improved relaxation) are selected to investigate the time dependent behavior of the numerical models. According to CEB-fib-2010 prediction model code, the relaxation after 1000 h (r_{1000}) was determined 0.04 and 0.06 for normal circumferential and vertical tendons; this parameter was reduced to 0.0123 and 0.01812 for improved ones. Prediction model codes, such as ACI 209R-92, Bažant-Baweja B3, CEB MC90-99, CEB-fib-2010 and BPEL-91 [3–7,20], are implemented to investigate the long-term prestress losses. Therefore, using five prediction models by considering three variable parameters in three categories of shrinkage & creep losses, stress relaxation losses and simultaneous losses, entirely 90 numerical models are compared to develop a long-term prestress loss interaction model. Eqs. (7) and (8) are the basis of the modulus of elasticity variation versus time due to creep in CEB-fib-2010 [6].

$$J(t, t_0) = \frac{1}{E_{cmt_0}} + \frac{\varphi_{28}(t, t_0)}{E_{cm28}} \tag{7}$$

$$E_{cmt} = \frac{1}{J(t, t_0)} \tag{8}$$

where $J(t, t_0)$ is compliance at concrete age t when loading starts at age t_0 in 1/MPa, $J(t_0, t_0)$ is elastic compliance at concrete age t_0 when loading starts at age t_0 in 1/MPa, $\varphi_{28}(t, t_0)$ is 28-day creep coefficient, E_{cmt_0} is mean modulus of elasticity of concrete when loading starts at age t_0 in MPa, E_{cm28} is mean modulus of elasticity of concrete at 28 days in MPa and E_{cmt} is mean modulus of elasticity of concrete at age t in MPa which is used as input data in property module of ABAQUS software [17].

The shrinkage strain development with time can be explained by Eqs. (9)–(11) in CEB 2010.

$$\epsilon_{sh}(t, t_c) = \epsilon_{cas}(t) + \epsilon_{cds}(t, t_c) \tag{9}$$

$$\Delta t = \frac{\epsilon_{sh}(t, t_c)}{\alpha} \tag{10}$$

$$T = 20 + \Delta t \tag{11}$$

where $\varepsilon_{sh}(t, t_c)$ is the shrinkage strain at concrete age t since the start of drying at age t_c in mm/mm, $\varepsilon_{cas}(t)$ is the autogenous shrinkage strain at concrete age t in mm/mm, $\varepsilon_{cds}(t, t_c)$ is the drying shrinkage strain at concrete age t since the start of drying at age t_c in mm/mm, α is the concrete thermal expansion coefficient in 1/°C, Δt is temperature difference in °C and

T is ABAQUS input data in °C. Indeed the shrinkage strains are converted to temperature type input data.

The calculation procedure of tendon stress relaxation resembles concrete shrinkage and can be described by Eqs. (12)–(15).

$$\rho_t = \rho_{1000}\left(\frac{t}{1000}\right) \tag{12}$$

$$\Delta\sigma = \sigma_0 \times \rho_t \tag{13}$$

$$\Delta t = \frac{\Delta\sigma}{(E_p \times \alpha)} \tag{14}$$

$$T = 20 + \Delta t \tag{15}$$

where ρ_t is relaxation after t hours, ρ_{1000} is relaxation after 1000 h, t is time in hours, t' is time in days, $\Delta\sigma$ is stress relaxation in MPa, σ_0 is initial stress in MPa, α is the tendon thermal expansion coefficient in 1/°C, E_p is the tendon modulus of elasticity in MPa, Δt is the temperature difference in °C and T is the ABAQUS input data in °C.

Long-term prestress losses are obtained based on averaging the tendon elements stress for vertical and horizontal ones in each time step. Eventually, 60 interaction coefficients are obtained.

7. FE modeling of the prestressed containment vessels

Long-term prestress losses are estimated using ABAQUS Standard [17]. C3D8R elements are chosen for solid elements of concrete. Prestressed and non-prestressed reinforcing are modeled using T3D2 elements. Embedded region technique is applied to define the interaction between concrete and steel. Fig. 2 explains the overall description of this technique.

Prestressing is applied by means of a predefined field in type of stress. To complete the prestressing definition, post-tensioning state was introduced to ABAQUS with a python command (*Prestress Hold). "Field Variables" is the most significant capability for investigation of prestress losses due to creep. The effective modulus of elasticity can be modified in each time steps through the field variables. Eqs. (7) and (8) can be utilized to calculate the effective modulus of elasticity input data based on CEB 2010 [6]. Since the temperature condition is assumed to be constant in inner and outer surfaces, no thermal Flux or Conduction forms through the wall thickness. Therefore, a predefined field with the type of temperature is used to define the thermal condition [17].

The stress relaxation losses can be rewritten in a simple form as ($\Delta f_{relaxation} = E_p \alpha \Delta T$). Thus, stress relaxation variation with time can be replaced by temperature variations. The temperature predefined field variable is implemented to apply different temperature to tendon elements at each time step. A similar procedure is performed to determine the shrinkage effects to the models.

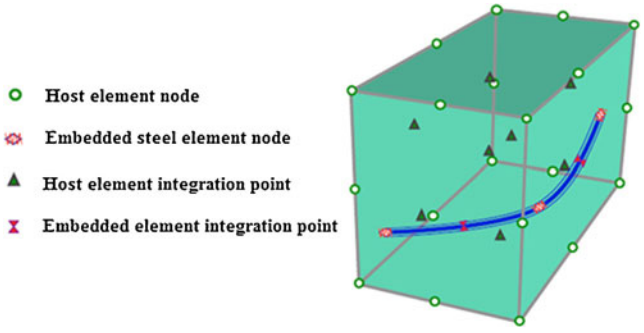

Fig. 2 – Embedded region technique [17].

8. Prestressed concrete containment vessel experiment

The prestress loss measurements were performed on the cylindrical prestressed concrete containment which was constructed at Amirkabir University of Technology (AUT). This experimental study was designed to verify the numerical analysis method. The test model geometric properties are presented next to the numerical model in Figs. 3 and 4. The test model consists of a cylindrical prestressed containment with six vertical and two circumferential post-tensioning tendons. The mix proportion of concrete is given in Table 6.

The Poisson's ratio was determined using the circumferential and axial extensometers mounted on concrete cylindrical specimens of size 150 mm diameter and 300 mm height. According to ASTM C469 [21], these parameters are obtained from Eqs. (16) and (17):

$$E = \frac{(S_2 - S_1)}{(\epsilon_2 - 0.000050)} \tag{16}$$

$$\nu = \frac{(\epsilon_{t2} - \epsilon_{t1})}{(\epsilon_2 - 0.000050)} \tag{17}$$

where E is the modulus of elasticity in MPa, S_2 is applied stress at 40 percent of ultimate loading in MPa, S_1 is applied stress concurrent with the longitudinal strain of value 0.000050 in MPa, ε_2 is longitudinal strain at S_2, ν is the Poisson's ratio, ε_{t2} is transverse strain in the middle of the sample at S_2, and ε_{t2} is transverse strain in the middle of the sample at S_1. According to the test results, the average value of 35.04 GPa was obtained

Table 6 – Concrete mix design.

Material (kg)	Mix proportions (kg/m^3)
Cement	430
Fine aggregate	985
Coarse aggregate	643
Limestone filler	110
Admixture	2.5
Water	163.4
Total	2334

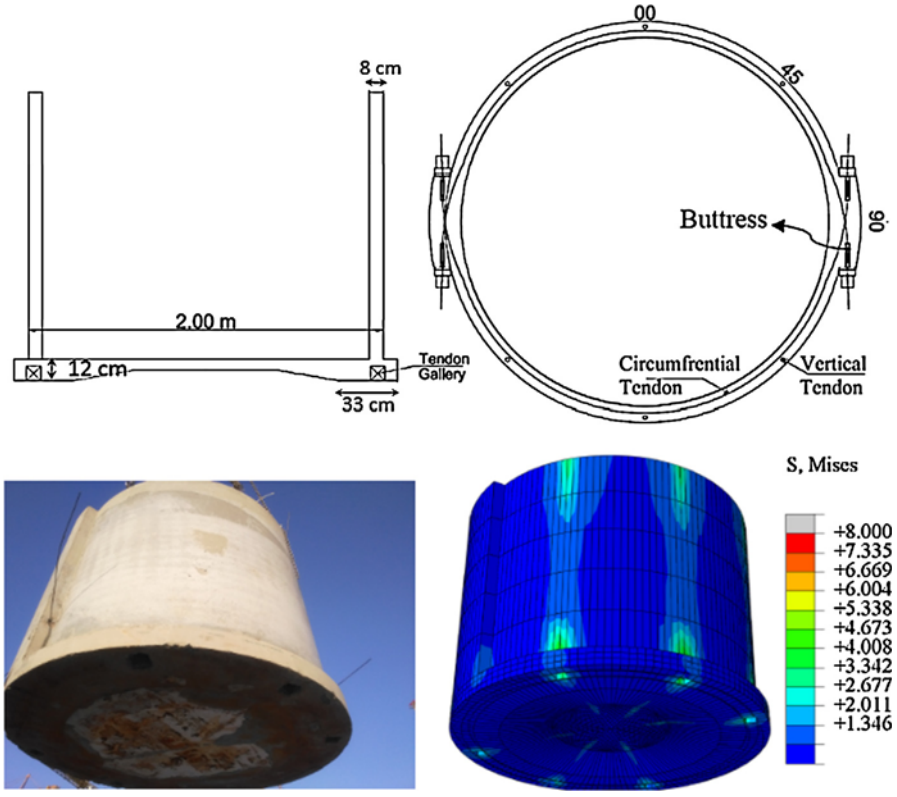

Fig. 3 – Geometry of AUT containment test model next to numerical model (S, Mises stress contour in MPa).

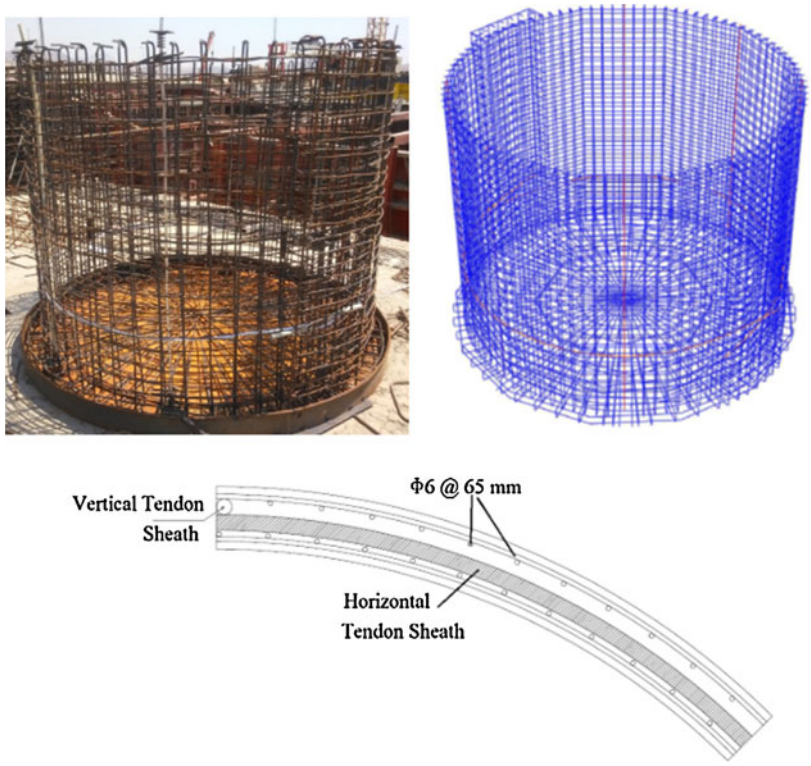

Fig. 4 – Reinforcement details of AUT containment test model next to numerical model.

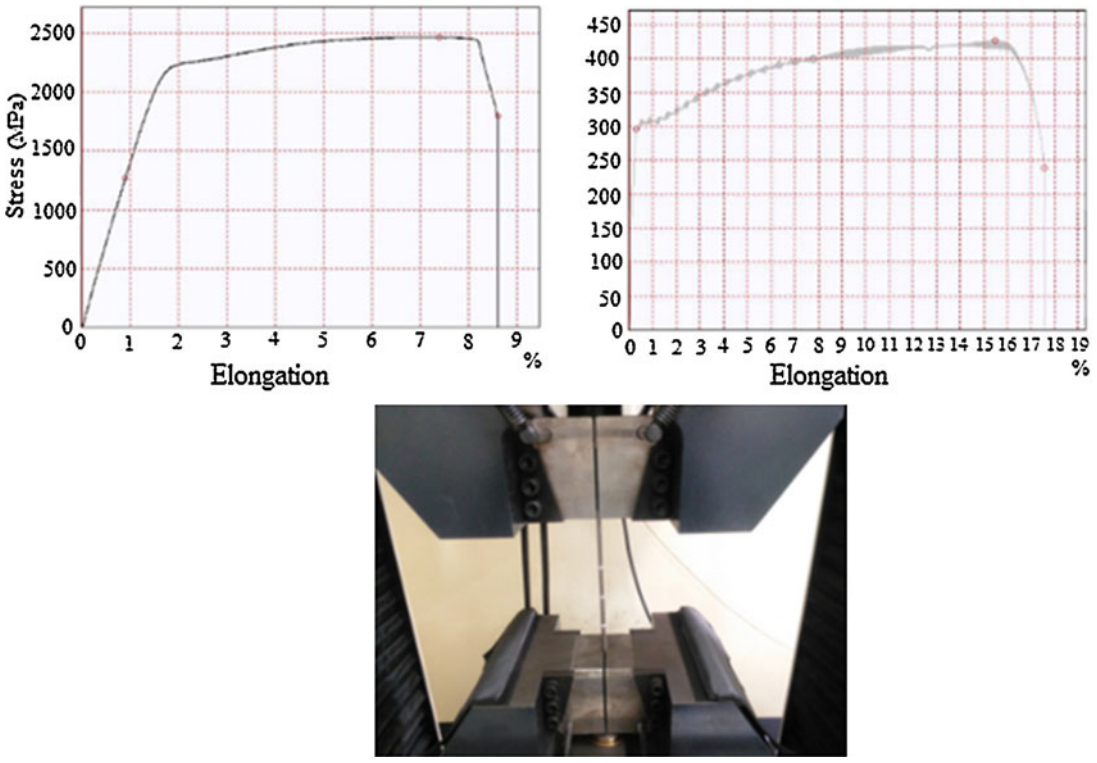

Fig. 5 – Tendon tensile test set up and sample results.

for the modulus of elasticity. The compressive strength test was repeated on three cubic specimens to ensure the test results. The average value of 48.3 MPa was achieved for the cylindrical standard compressive strength in both series of specimens.

So closed distance between the reinforcement bars govern the concrete SCC type to fill everywhere in the cylindrical test model. The core wire of 1/2 in seven wire strand was implemented to apply prestressing in the containment test model. The ultimate tensile test set up and its results for the selected prestressing wire and reinforcing bars are shown in Fig. 5. Three specimens of length 400 mm were provided for each of the prestressed and non-prestressed reinforcement. The fixed and movable grip faces of tensile test machine were selected due to the sample diameter. The result sheet was printed automatically after tensile rupture of the samples.

The Poisson's ratio for both prestressed and non-prestressed reinforcing is 0.3. The modulus of elasticity for steel reinforcement and tendons are 146 GPa and 143 GPa, respectively. The ultimate strength value of reinforcing bars and tendons are 427 MPa and 2464 MPa.

A special integrated cylindrical concrete form was required to cast the SCC concrete in the containment thin wall and its foundation simultaneously. The concrete form was designed to endure upward pressure of the concrete to upper part of the concrete form in the foundation.

At first, external wall sheet and bottom part of the foundation concrete form was bolted to each other tightly. The tendon sheaths and the non-prestressed reinforcement cage were attached to the concrete forms according to the shop drawings exactly. Then inner part of the wall concrete forms were installed and welded to the outer part. In addition, some channel-section struts were used to prevent the upward motion of the inner part. Two lens shapes pieces were fixed on the bottom plate of the foundation mold to form a circular foundation with variable section. At the bottom of the test model, six cubic wooden parts were stuck on the foundation mold plate to serve some spaces as tendon galleries as illustrated in Fig. 6. Finally, all of the concrete form edges were filled with concrete foam. Fig. 6 illustrates the different parts of the test model concrete form.

The concrete components were mixed by means of the batching plant and were placed using a hand created pocket and V-funnel to fill the thin wall of the test model. The total volume of the fresh concrete was about 1.2 m^3. The concrete forms were released after 24 h and the test model was cured for 7 days by drenched gunny cloth.

The tendon force was measured by lifting the anchor head using a prestressing jack and recording when the anchor head started to move, a so-called lift-off test. Measurements were performed on both circumferential and vertical tendons at 232 days after loading age. Fig. 7 illustrates the post-tensioning procedure of the test model.

The additional input data required for the prediction models are listed in Table 7. The results in Tables 8 and 9 show that the prediction models estimate the measured prestress losses fairly. There is a better agreement between measured and calculated losses in the vertical direction, which probably is due to the influence of friction and force redistribution on the circumferential tendons. The

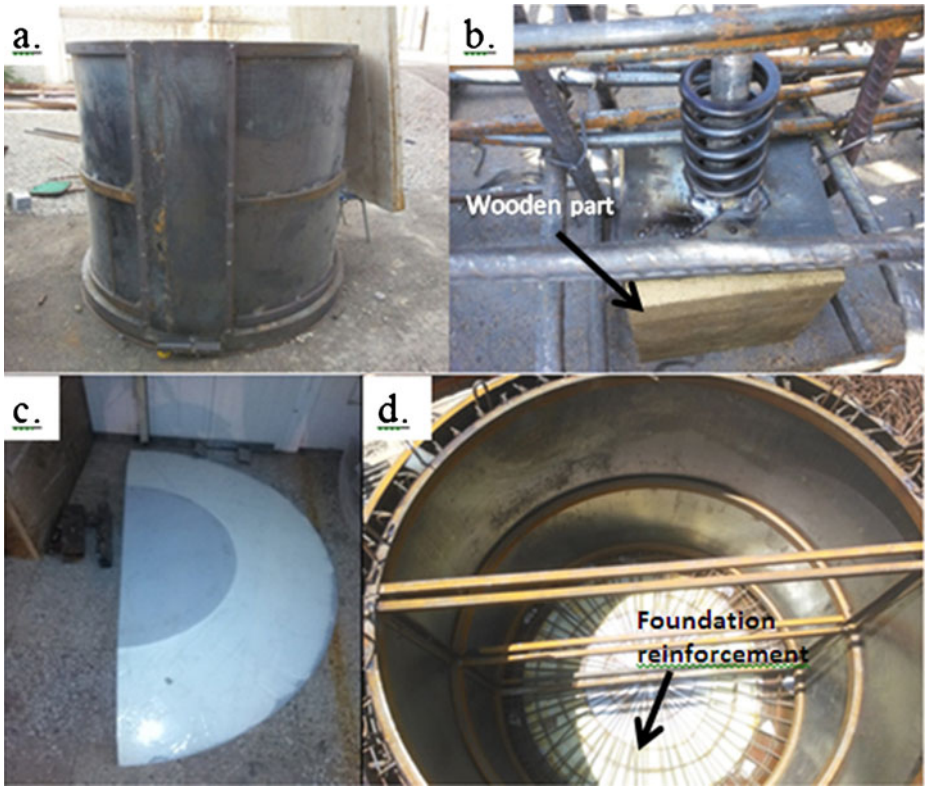

Fig. 6 – Prestressed containment test model concrete form. (a) outer form of wall; (b) cubic wooden part for creating an empty space for tendon gallery; (c) lens shape partition for making the foundation thickness variation; (d) upward view before the upper part of the foundation form installation.

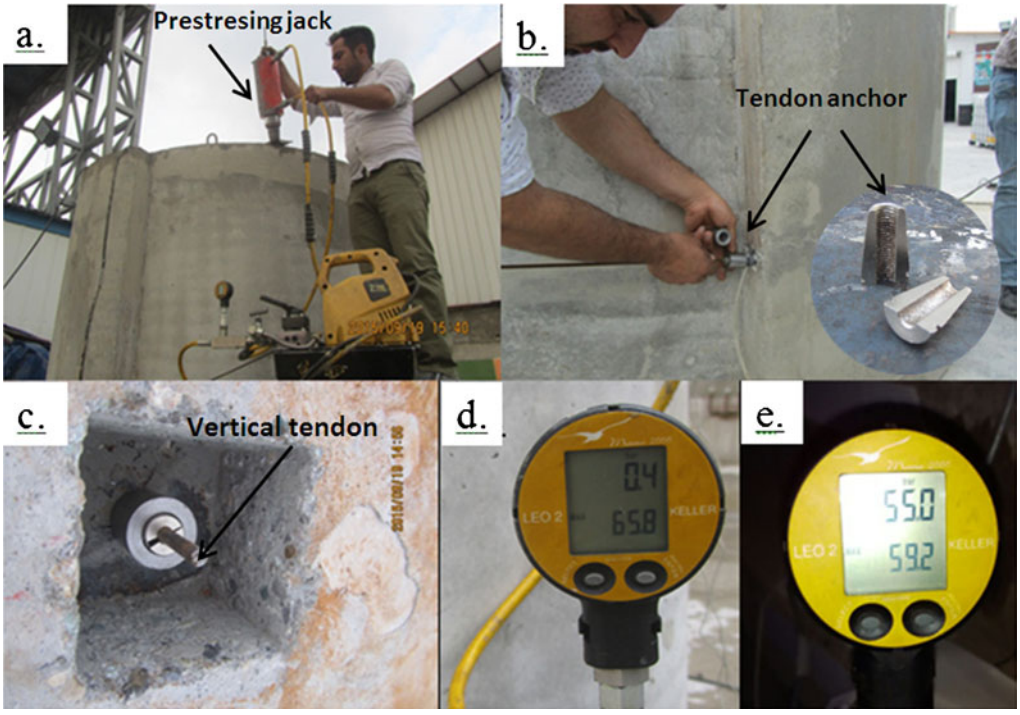

Fig. 7 – Tendon post-tensioning process. (a) vertical tendon tensioning; (b) circumferential tendon anchors; (c) vertical tendon gallery in the bottom of the foundation; (d) manometer display for vertical tendons at first time of the tensioning; (e) pressure gauge display for vertical tendons in the lift-off.

Table 7 – Input parameters for prediction models.

Parameter	Value
Curing time (days)	7
Age at loading (days)	42
Compressive strength (MPa)	48.3
Elastic modulus (GPa)	35.04
Poisson's ratio	0.207
Volume/surface ratio (mm)	40
Relative humidity	0.7
Temperature	20
Maximum aggregate size (mm)	8.5
Water-cement (W/C)	0.38
Aggregate-cement (a/c)	4.041
Fine aggregate percentage, Ψ (%)	46.91
Air content, α (%)	2
Slump (mm)	>130
Unit weight (kg/m^3)	2635

comparison of the results demonstrates that the predictions by CEB/FIB 2010 and CEB/FIP 99 [5,6] present the closest results to the measured values.

9. Results and discussions

Several key parameters such as dimensional proportion, temperature and tendon material (normal or improved relaxation) are investigated to estimate the long-term prestress losses in circular containments. The analysis results illustrate that the long-term prestress loss values are independent from (R/H) ratio. Study of prestressing variations for 30 years indicate that dimensional proportion does not have any significant effect on the time dependent behavior, even in the presence of temperature and tendon material variables.

The diverse initial prestressing force of the numerical models caused to the little difference between the results in Figs. 8 and 9. As depicted in Figs. 8–11, the long-term prestress losses increment with time at former times, especially the first 1000 days is considerably higher than other times. The comparison of Figs. 8 and 10 demonstrate that the vertical prestressing long-term losses are less than the circumferential prestressing. This difference is reduced for the improved tendons as illustrated in Figs. 9 and 11. The difference between the models with temperature effects is less than the others. The trend in these figures indicates a significant effect of temperature in the prestress loss. The temperature effects are gradually increased in both normal and improved relaxation tendons.

Figs. 12 and 13 illustrate the comparison of the prestress losses due to creep and shrinkage with and without temperature effects in various prediction models. As it can be seen in these figures, the main prestress losses portion due to creep and shrinkage take place at the earliest ages.

BPEL-91 code [20] provides the maximum prestress loss prediction due to creep and shrinkage and the minimum values belong to CEB-2010 model code [6]. CEB MC90-99 and CEB-2010 [5,6] give same values for the creep and shrinkage losses, but by considering the temperature effects CEB MC90-99 [5] concludes with higher results.

Figs. 14 and 15 illustrate prestress losses due to the stress relaxation using different methods. The comparison of Figs. 14 and 15 with Figs. 8–11 demonstrate that the variation of the relaxation prestress losses has a same trend as the total time dependent losses. According to the obtained results, it can be seen that the improved relaxation tendon will reduce the stress relaxation prestress loss by more than 50 percent in both BPEL-91 [20] and CEB-2010 methods [6]. Implementation of the improved relaxation tendon material decreases the relaxation prestress losses due to temperature conditions by 40 percent.

Table 8 – Measured and calculated horizontal tendons losses.

Prediction model	Jacking stress	Effective prestressing after losses	Total losses in percent	Short-term losses	Long-term losses
ACI	1774.3185	1389.64	21.68	12.77	8.91
B3	1774.3185	1410.46	20.51	12.77	7.74
CEB-99	1774.3185	1431.1	19.34	12.77	6.58
CEB-2010	1774.3185	1431.28	19.33	12.77	6.57
BPEL	1774.3185	1416.73	20.15	12.77	7.39
Measured (upper limit)	1774.3185	1458.34	17.81	–	–
Measured (lower limit)	1774.3185	1482.65	16.44	–	–

Table 9 – Measured and calculated vertical tendons losses.

Prediction model	Jacking stress	Effective prestressing after losses	Total losses in percent	Short-term losses	Long-term losses
ACI	1599.3172	1361.43	14.87	3.16	11.71
B3	1599.3172	1385.31	13.38	3.16	10.22
CEB-99	1599.3172	1406.89	12.03	3.16	8.87
CEB-2010	1599.3172	1408	11.96	3.16	8.80
BPEL	1599.3172	1393.96	12.84	3.16	9.68
Measured (upper limit)	1599.3172	1434.038217	11.24	–	–
Measured (lower limit)	1599.3172	1446.191083	9.57	–	–

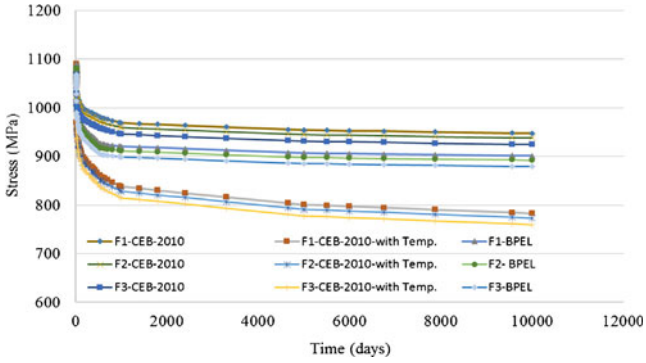

Fig. 8 – Long-term prestress loss in circumferential tendons (normal relaxation).

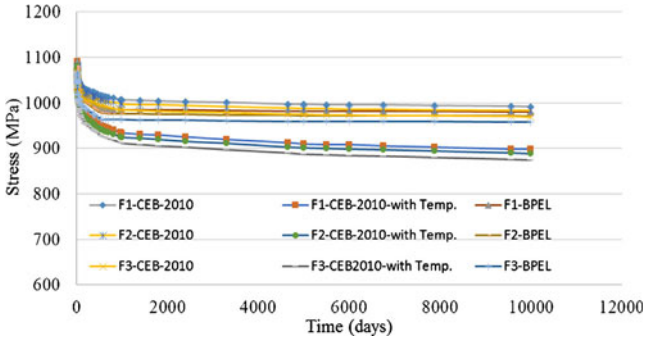

Fig. 9 – Long-term prestress loss in circumferential tendons (improved relaxation).

Fig. 16 displays the stress contour in CEB-2010 model code [6] with and without temperature effects. The temperature effects were observed on the ultimate value of prestressing and stress distribution along the tendon. The superposition of the separate prestress losses provides different values than the losses due to the simultaneous application of all factors. BPEL-91 [20] offers an interaction coefficient to consider the interaction of concrete creep and tendon stress relaxation in the step by step prestress loss calculation method.

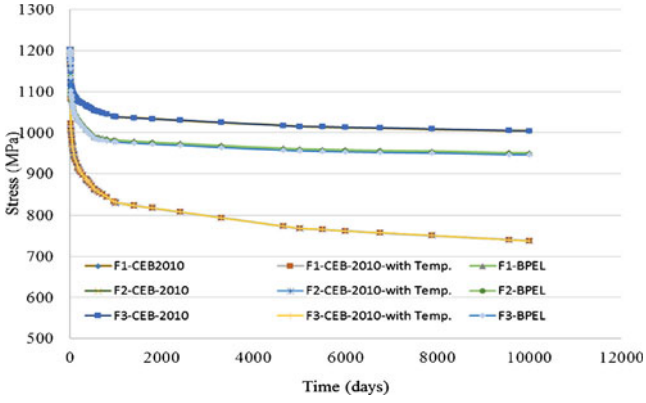

Fig. 10 – Long-term prestress loss in vertical tendons (normal relaxation).

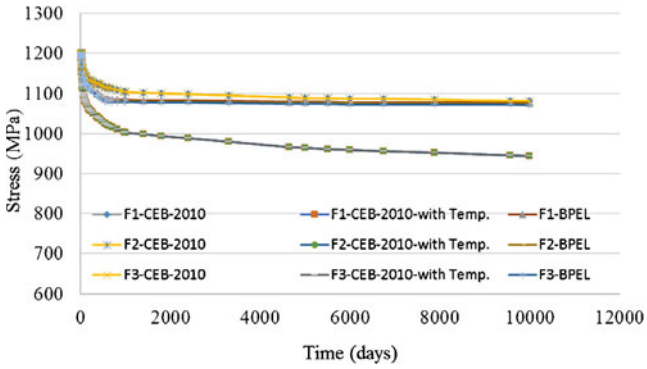

Fig. 11 – Long-term prestress loss in vertical tendons (improved relaxation).

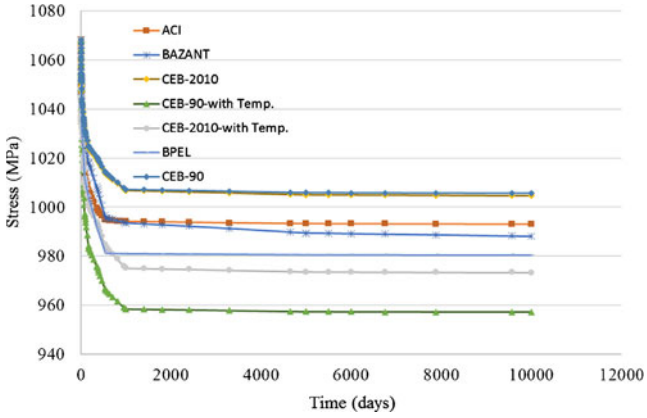

Fig. 12 – Prestress loss due to creep and shrinkage in circumferential tendons (model F-3).

$$\Delta = \Delta_1 + \Delta_2 + \Delta_3 + \Delta_4 + \Delta_5 + \frac{5}{6}\times\Delta_6 \tag{18}$$

where Δ_1–Δ_6 are prestress losses due to anchorage slip, elastic shortening of concrete, friction, shrinkage of concrete, creep of concrete and tendon relaxation, respectively. The interaction coefficient was obtained for all of the cases described above to precisely correct Eq. (18) for prestress loss prediction of circular prestressed containment vessels. Tables 10 and 11 summarize the interaction coefficient results for model F3.

As previously discussed about Figs. 8–11, the ultimate long-term prestress losses for models F1 and F2 are same as the values in Tables 10 and 11. BPEL-91 and CEB-99 estimate the greatest and the smallest ultimate long-term prestress loss for normal relaxation tendons among the prediction models. The average amount of the ultimate prestress loss in the vertical tendons is about 27.5 percent more than the circumferential tendons. The reason can be explained by the different distance of the vertical and horizontal tendons and the different compressive stress produced in concrete by these tendons. The different initial prestressing force may be contributed to the greater long-term prestress loss.

Table 12 presents the interaction coefficients for all models in vertical and circumferential tendons. As it can be calculated

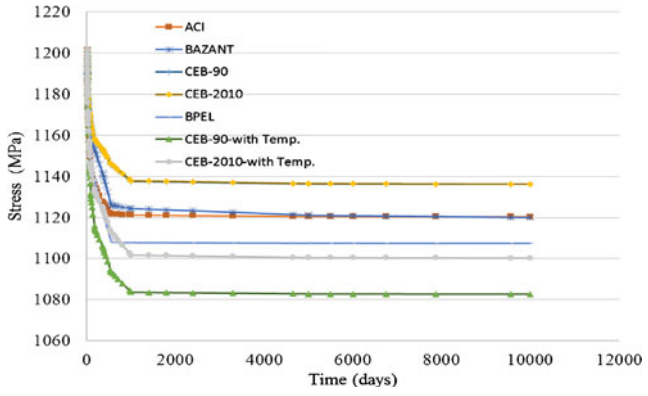

Fig. 13 – Prestress loss due to creep and shrinkage in vertical tendons (model F-3).

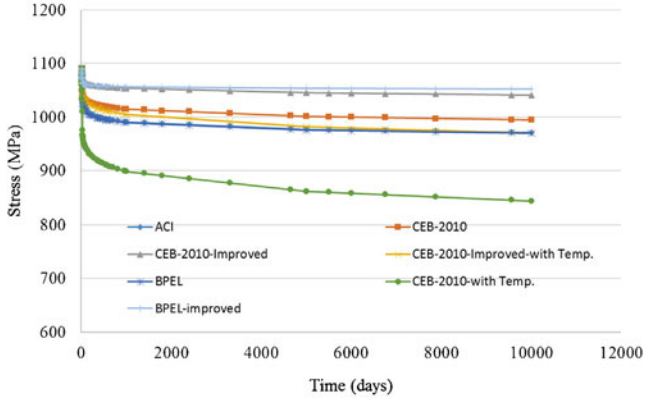

Fig. 14 – Prestress loss due to relaxation in circumferential tendons (model F1).

from Table 12 coefficients, the average difference between the interaction coefficients of the models is about 1.15 percent and 2.99 percent for circumferential and vertical tendons, respectively. Therefore, this parameter can be ignored in interaction coefficient calculations.

The numerical study results demonstrate that the average value of the interaction coefficient for vertical tendons is 9.32 percent more than horizontal tendons. In fact the greater

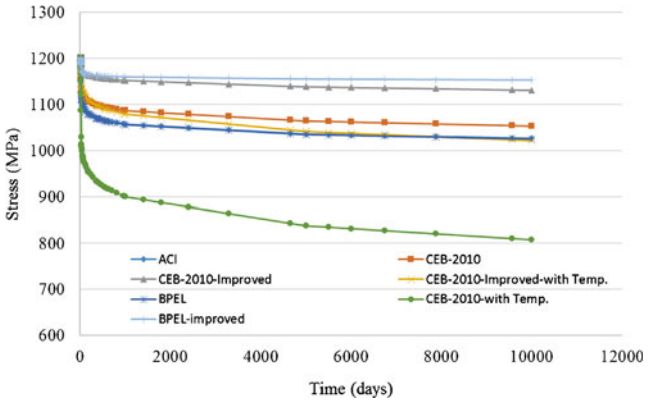

Fig. 15 – Prestress loss due to relaxation in vertical tendons (model F1).

long-term prestress loss in vertical direction leads to the greater interaction coefficients. Diverse variables were investigated to attain a determinant method for estimation of the interaction coefficient. By comparison of the interaction coefficient values in various methods, it can be found that the interaction coefficients were amplified by increasing stress relaxation losses in relation to creep and shrinkage losses ($\Delta_6/(\Delta_4+\Delta_5)$). Fig. 17 shows the interaction coefficient variations due to the ratio of ($\Delta_6/(\Delta_4+\Delta_5)$).

As illustrated in Fig. 17, Eq. (19) was obtained using the best trend curve over the interaction coefficients. Accordingly, Eq. (20) is recommended in two limits to achieve the best consistency between the estimated values and the current study results, where x is the interaction coefficient.

$$x = 0.1491\times\ln\left(\frac{\Delta_6}{\Delta_4+\Delta_5}\right)+0.7678 \tag{19}$$

$$\begin{cases} \dfrac{\Delta_6}{\Delta_4+\Delta_5}\le 1.3 \Rightarrow x = 0.0866\times\ln\left(\dfrac{\Delta_6}{\Delta_4+\Delta_5}\right)+0.8166 \\ \dfrac{\Delta_6}{\Delta_4+\Delta_5} < 1.3 \Rightarrow x = 0.2004\times\ln\left(\dfrac{\Delta_6}{\Delta_4+\Delta_5}\right)+0.7723 \end{cases} \tag{20}$$

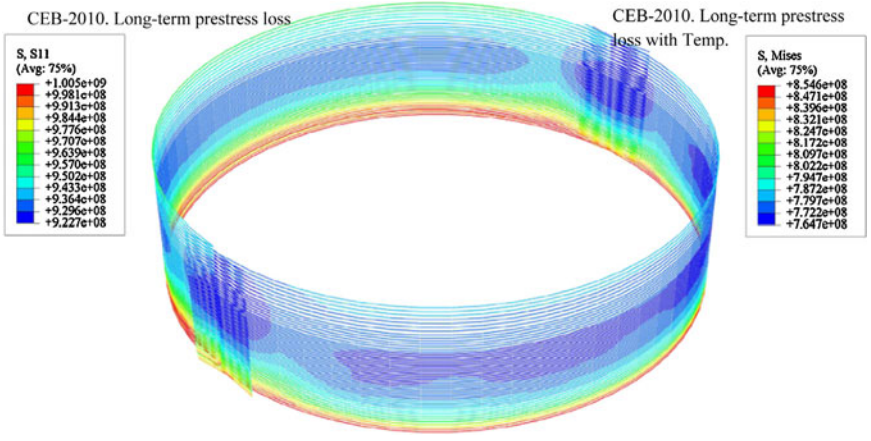

Fig. 16 – Stress contour in circumferential tendons for normal relaxation tendon [17].

Table 10 – Interaction coefficient for creep, shrinkage and relaxation effects in circumferential tendons of model F3.

Models	Creep and shrinkage losses (MPa)	Relaxation losses (MPa)	Simultaneous losses (MPa)	Interaction coeff.
Long-term prestress losses in circumferential tendons (normal relaxation)				
ACI	75.111	120.466	177.63	0.8510202
BAZANT	80.044	120.466	180.505	0.8339365
CEB-99	63.53	96.503	143.894	0.8327617
CEB-2010	63.54	96.503	143.855	0.8322539
CEB-99-T	110.941	247.492	319.528	0.842803
CEB-2010-T	94.775	247.492	308.198	0.862343
BPEL-91	87.598	121.97	188.95	0.8309584
Long-term prestress losses in circumferential tendons (improved relaxation)				
CEB-2010	63.54	50.35	98.592	0.6961668
CEB-2010-T	94.775	121.69	193.169	0.8085627
BPEL-91	87.598	40.71	110.108	0.5529354

Table 11 – Interaction coefficient for creep, shrinkage and relaxation effects in vertical tendons of model F3.

Models	Creep and shrinkage losses (MPa)	Relaxation losses (MPa)	Simultaneous losses (MPa)	Interaction coeff.
Long-term prestress losses in vertical tendons (normal relaxation)				
ACI	81.08	177.14	243.352	0.9160664
BAZANT	81.49	177.14	242.133	0.9068703
CEB-99	65.24	148.41	197.34	0.8901017
CEB-2010	65.25	148.41	197.31	0.8898322
CEB-99-T	118.82	393.516	476.517	0.908977
CEB-2010-T	101.16	393.516	463.447	0.9206411
BPEL-91	94.05	178.29	255.431	0.9051601
Long-term prestress losses in vertical tendons (improved relaxation)				
CEB-2010	65.25	70.61	120.32	0.7799179
CEB-2010-T	101.16	180.55	257.932	0.8683024
BPEL-91	94.05	50.93	129.91	0.7041037

Table 12 – (R/H) ratios effects on interaction coefficient.

Model	Circumferential tendons			Vertical tendons		
	F1	F2	F3	F1	F1	F3
ACI	0.865	0.855	0.851	0.928	0.923	0.916
BAZANT	0.852	0.841	0.834	0.920	0.914	0.907
CEB-99	0.844	0.840	0.833	0.920	0.904	0.890
CEB-2010	0.843	0.837	0.832	0.920	0.904	0.890
CEB-99-T	0.842	0.842	0.843	0.927	0.915	0.909
CEB-2010-T	0.861	0.862	0.862	0.935	0.927	0.921
BPEL-91	0.847	0.837	0.831	0.919	0.913	0.905
Improved relaxation tendons						
CEB-2010	0.717	0.706	0.696	0.843	0.810	0.780
CEB-2010-T	0.807	0.807	0.809	0.901	0.881	0.868
BPEL-91	0.581	0.560	0.553	0.739	0.723	0.704

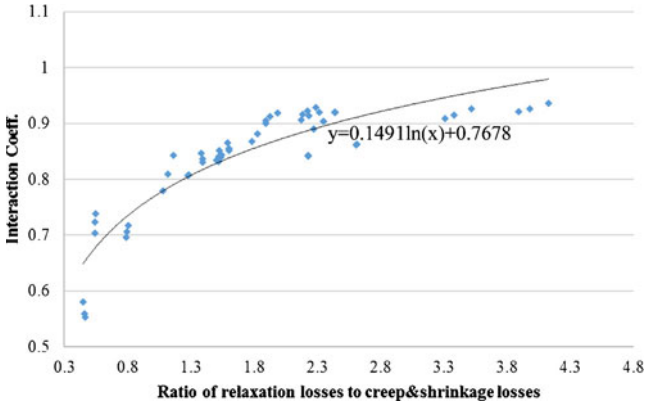

Fig. 17 – Interaction coefficient variations in relation to the ratio of stress relaxation losses to creep and shrinkage losses.

10. Conclusions

Tendon prestress losses include short-term prestress losses and long-term prestress losses. The short-term prestress losses consist of anchorage slip, elastic shortening and friction (Δ_1, Δ_2, Δ_3) and the long-term prestress losses include shrinkage, creep and stress relaxation (Δ_4, Δ_5, Δ_6). Conventionally, in order to predict the long-term losses, prestress losses are computed separately. Following, the total losses can be obtained using the superposition principle.

In order to estimate long-term prestress losses in prestressed concrete containment vessels, three main variables including dimensional proportion (R/H), constant temperature condition, and tendon material (normal or improved relaxation) were considered using five prediction models. The numerical results over 30 years demonstrated that the long-term prestress loss values are independent of the dimensional proportion (R/H) ratio.

The maximum and minimum prediction of creep and shrinkage prestress losses were achieved based on BPEL-91 [20] and CEB-2010 model code [6], respectively. It can be observed that CEB MC90-99 and CEB-2010 [5,6] provides the same results for creep and shrinkage losses except for models with temperature conditions. Additionally, the stress relaxation prestress loss is reduced by more than 50 percent using the improved relaxation tendon material. Concerning the temperature conditions, the stress relaxation prestress losses are increased for the normal tendon material by 40 percent more than the improved ones.

The main contribution of this study is to formulate the interaction effects between the concrete creep and tendon relaxation losses. In doing so, a series of numerical analyses were performed to consider the effective variables in long-term prestress losses to express the interaction coefficient (x) as a function of ($\Delta_6/(\Delta_4 + \Delta_5)$). The results show that the average value of the interaction coefficient for circumferential tendons is 9.32 percent less than vertical ones. The interaction coefficients can be magnified by increasing the ratio of stress relaxation losses to creep and shrinkage losses ($\Delta_6/(\Delta_4 + \Delta_5)$).

REFERENCES

[1] Z.P. Bazant, Numerical determination of long-range stress history of strain history in concrete, Materials and Structures 5 (3) (1972) 135–141.

[2] Z.P. Bazant, Prediction of concrete creep effects using age adjusted effective modulus method, ACI Journal 69 (20) (1972) 212–217.

[3] American Concrete Institute (ACI) Committee 209, Guide for Modeling and Calculating Shrinkage and Creep in Hardened Concrete, ACI Report 209.2R-08, American Concrete Institute, Farmington Hills, MI, 2008.

[4] Comité Euro-international du béton-Fédération Internationale de la précontrainte (CEB-FIP), Model Code for Concrete Structures, Thomas Telford Services Ltd., London, 1990.

[5] Fédération Internationale du Béton (fib), Structural Concrete: Textbook on Behavior, Design and Performance, Updated Knowledge of the CEB/FIP Model Code 1990, Bulletin No. 2, Vol. 1, Fédération Internationale du Béton, Lausanne, Switzerland, 1999.

[6] CEB-FIP, fib Model Code for Concrete Structures, Ernst & Sohn Publishing House, Berlin, 2010.

[7] Z.P. Bazant, S. Baweja, Creep and shrinkage prediction model for analysis and design of concrete structures: Model B3, in: A. Al-Manaseer (Ed.), Adam Neville Symposium: Creep and Shrinkage – Structural Design Effects, ACI SP-194, American Concrete Institute, Farmington Hills, MI, 2000 1–83.

[8] Z.P. Bazant, M.H. Hubler, M. Jirásek, Improved Estimation of Long-Term Relaxation Function from Compliance Function of Aging Concrete, Journal of Engineering Mechanics 139 (2013) 146–152.

[9] T.K. Francis, X.T. Si, Accurate time-dependent analysis of concrete bridges considering concrete creep, concrete shrinkage and cable relaxation, Engineering Structures 33 (2011) 118–126.

[10] P. Lundqvist, L.O. Nilsson, Evaluation of prestress losses in nuclear reactor containments, Nuclear Engineering and Design 241 (2011) 168–176.

[11] T.H. Hsuan, J.X. Lin, Ultimate analysis of PWR prestressed concrete containment under long-term prestressing loss, Annals of Nuclear Energy 87 (2016) 500–510.

[12] American Concrete Institute (ACI) Committee 372, Design and Construction of Circular Wire and Strand Wrapped Prestressed Concrete Structures, ACI Report 372R.00, American Concrete Institute, Farmington Hills, MI, 2000.

[13] SAP 2000 Inc, Integrated Finite Element Analysis and Design of Structures – Software, Computers and Structures Inc., Berkeley, CA, USA, 2015.

[14] ASCE Standard ASCE/SEI 7-16, Minimum Design Loads for Buildings and Other Structures, American Society of Civil Engineering, 2016.

[15] ASCE Standard ASCE/SEI 41-13, Seismic Evaluation and Retrofit of Existing Buildings, American Society of Civil Engineering, 2016.

[16] G. Nawy, Prestressed Concrete – A Fundamental Approach, Pearson Education, Inc., Upper Saddle River, New Jersey, 2010.

[17] ABAQUS Inc., ABAQUS 6.14 Analysis User's Manual, SIMULIA, 2014.

[18] M.F. Hessheimer, R. Dameron, Containment Integrity Research at Sandia National Laboratories, Division of Fuel, Engineering & Radiological Research, Office of Nuclear Regulatory Research, US Nuclear Regulatory Commission, 2006.

[19] A. Naaman, Prestressed Concrete Analysis and Design, McGraw-Hill Publishing Company, San Francisco, 1989.

[20] Regies techniques de conception et de calcul des ouvrages et construction en beton precontraint suivant la methode des etats limites: BPEL 91 revise 99, Eyrolles, France, 1999.

[21] ASTM C469, Standard Test Method for Static Modulus of Elasticity and Poisson's Ratio of Concrete in Compression, Annual Book of ASTM Standards, West Conshohocken, PA, U.S.